ACS OMEGA

Open Access

http://pubs.acs.org/journal/acsodf

Article

Investigation into the Dissolution Kinetics of Different MgO Desulfurizers in Flue Gas Desulfurization

Mengyu Ma,* Hongge Zhao, and Peng Hu

Cite This: *ACS Omega* 2024, 9, 12779−12788

Read Online

ACCESS | Metrics & More | Article Recommendations

ABSTRACT: The paper introduced hydrophilic functional groups on the surface of the MgO desulfurizer to improve its dispersion and hydrophilicity on the basis of reducing the particle size of the MgO desulfurizer to the nanometer level. Mechanical grinding technology was used to improve the traditional two-step method to lay the foundation for its large-scale production. The stability test showed that the ζ potential of the 5 wt % modified MgO desulfurizer was greater than 50 mV with 30 days of storage, and the sedimentation rate was not more than 7%. The dissolution reactivity and kinetics experiments showed that the decrease of particle size and the increase of hydrophilicity and dispersion were conducive to accelerating the dissolution rate of the MgO desulfurizer and reducing the apparent activation energy. Meanwhile, the good dissolution rate of the modified MgO nanofluids prepared by the improved method could reduce the liquid film mass transfer resistance and prolonged the penetration time.

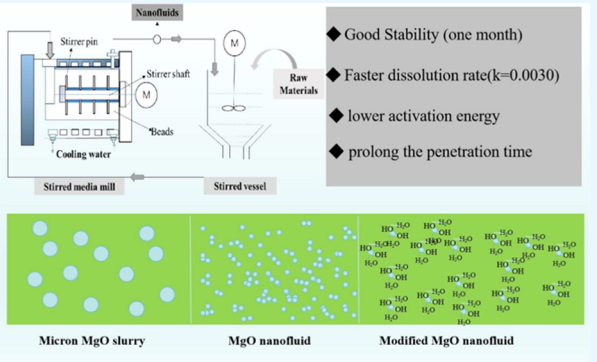

1. INTRODUCTION

SO_2 in the flue gas from coal combustion has become the main cause of air pollution. Large-scale researches are carried out to control SO_2 emissions, of which flue gas desulfurization technology is the most commonly used method to reduce SO_2 emissions.[1−4] The most mature flue gas desulfurization method is the limestone−gypsum method, but its shortcomings are also prominent. Large investment, high energy consumption, and easy blockage of equipment restrict its development space.[5,6] Compared with the limestone method, MgO flue gas desulfurization technology has a higher desulfurization effect, a lower equipment investment and operation cost, and is not easy to block, which has been the focus of research and development in the domain of desulfurization.[7]

The removal of SO_2 by the MgO desulfurizer is a complex reaction process of gas, liquid, and solid phases, including the dissolution of MgO particles and the absorption of SO_2.[8] The dissolution of MgO particles is an important rate-determining step in the whole process, which has a significant impact on the whole desulfurization process.[9] Promoting MgO particle dissolution can not only enhance the absorption of SO_2 but can also reduce the residual amount in the byproduct and improve the quality of $MgSO_4$ byproducts. Currently, the dissolution of desulfurizers is mainly measured indirectly by acid titration, which is significantly different from the actual desulfurization process and cannot reflect the gas−liquid−solid three-phase reaction process.[10−12] There were few studies to explore the dissolution characteristics of MgO particles directly in the actual desulfurization process.[13,14]

Many scholars tried to study the influence of particle size and particle size distribution on flue gas desulfurization, and it was found that the dissolution rate of the solid desulfurizer decreased with the increase of particle size.[15] In recent years, with the development of nanotechnology, measures had been taken to reduce the particle size from micron to nanometer.[16−20] However, although the particle size of the nanoparticle is small and the specific surface energy is large, it is easy to agglomerate due to the high surface energy, which not only does not increase the gas−solid contact area but also causes blockage of the equipment due to the formation of precipitation.[21−25]

In order to solve the agglomeration of nanoparticles, researchers tried to improve the dispersion of nanoparticles in the basefluid by various methods without changing the properties of nanoparticles.[26,27] For example, multiwalled carbon nanotubes (MWCNTs) are extremely unstable in the basefluid and easy to curl up into clusters; Karami et al.[28]

Received: October 30, 2023
Revised: February 11, 2024
Accepted: February 19, 2024
Published: March 7, 2024

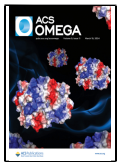

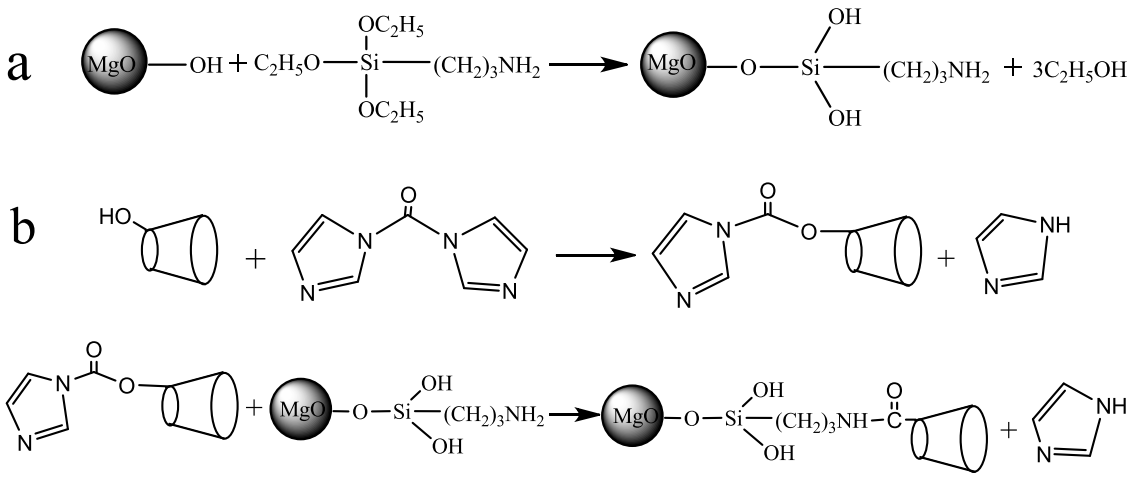

Figure 1. Synthesis route of the modification of MgO nanoparticles: (a) the synthetic route of aminopropyl−MgO and (b) the synthetic route of cyclodextrin-modified MgO nanoparticles.

improved their stability by functionalizing them with carboxyl groups. Said[29] treated carbon nanotubes with acid to increase the hydrophilic functional group on the surface of carbon nanotubes so that the nanofluid could be stable for three months. Xian et al.[30] compared the effects of six surfactants (PVP, Triton X-100, SDS, SDC, SDBS, and CTAB) on the stability of graphene−TiO_2 hybrid nanofluids and found that CTAB was the best surfactant to enhance the stability of hybrid nanofluids. Choudhary et al.[31] discovered that the stability of water-based Al_2O_3 nanofluids could be affected by pH and sonication time. They found that the dispersion of high-concentration nanofluids could be improved by increasing the ultrasonic oscillation time and the dispersion performance could be improved by increasing the acidity or alkalinity. It could be found that surface modification, ultrasonic oscillation, adjusting pH, and addition of surfactants could improve the stability of nanofluids. However, an acid or alkali environment would affect the desulfurization effect of desulfurizers. Moreover, the change of the surfactant structure at a certain temperature would affect the uniform dispersion of the desulfurizer. Therefore, surface modification provided the possibility to improve the stability of the nano-MgO nanofluid desulfurizer.

Although the researches on the practical application of nanofluids have drawn more and more attention, they are still in the primary stage.[32] Actually, the most fundamental problem is the preparation of nanofluids. In order to meet the demand of high dispersion and stability, the preparation process of nanofluids usually had low output and high energy consumption, which is difficult to implement on a large scale. The satisfaction of this demand has practical significance for the large-scale industrial application of nanofluids[33]. Mechanical milling had been used to prepare highly stable micron dispersions, which could be used in various industrial fields, such as food, pigments, and cosmetics.[26,34,] In addition, wet milling could usually be used in the industrial production of nanoparticles.[36] At present, few studies have linked it with the application of nanofluids. Unlike the two-step ultrasonic method for preparing nanofluids, mechanical grinding technology has sufficient potential to effectively expand the production scale of nanofluids.

Therefore, hydrophilic functional groups were introduced into the surface of MgO nanoparticles, and then mechanical grinding technology was used to achieve the large-scale preparation of a nano-MgO desulfurizer with high dispersion and stability. The particle size, ζ potential, and sedimentation rate of modified and unmodified nano-MgO desulfurizers prepared by mechanical grinding technology were measured to analyze their dispersion and stability. Then, the dissolution reactivity and desulfurization effect of these desulfurizers were studied; especially, the core shrinking model was introduced to closely analyze the influence of dispersion on the dissolution kinetics and desulfurization effect of the nano-MgO desulfurizer.

2. EXPERIMENTAL METHODS AND MATERIALS

2.1. Materials. MgO nanoparticles (diameter of 50 nm, purity >95%) were obtained from C.W. Nanotechnology Company (Shanghai, China). (3-Aminopropyl)triethoxysilane, 1,1-carbonyldiimidazole, and toluene were obtained from Adamas-β Reagent Co., Ltd. (Shanghai, China). β-Cyclodextrin and *N*,*N*-dimethylformamide (DMF) were obtained from Sinopharm Chemical Reagent Beijing Co., Ltd.

2.2. Preparation and Characterization of Modified MgO Nanoparticles. First, MgO nanoparticles were added into 100 mL of toluene under magnetic stirring and then suspended by ultrasonic treatment for 0.5 h. Then, 5 mL of (3-aminopropyl)triethoxysilane was mixed in the above solution and stirred for 6 h at 100 °C. Then, the mixture was cooled, filtered, washed with toluene and acetone, and dried. The aminopropyl−MgO mixture was prepared.

β-Cyclodextrin (6 g) was dissolved into *N*,*N*-dimethylformamide (100 mL), and then 6 mL of 1,1-carbonyldiimidazole was mixed into the solution. The hydroxyl group of cyclodextrin was activated by magnetic stirring for 2 h at 25 °C. The prepared aminopropyl−MgO mixture was suspended in DMF (100 mL), and then the solution containing activated β-cyclodextrin was slowly added into the suspension. The mixture was stirred for 20 h under magnetic force at 25 °C. Then, the product was washed with DMF, acetone, and deionized water to obtain cyclodextrin-modified MgO nanoparticles. The synthesis route of modified MgO nanoparticles is shown in Figure 1.

The structures of MgO nanoparticles and modified MgO nanoparticles were measured using an FTIR spectrometer (Nicolet Nexus 470, Nicolet). The spectrogram with the

https://doi.org/10.1021/acsomega.3c08575
ACS Omega 2024, 9, 12779−12788

wavelength ranging from 4000 to 500 cm^{-1} was recorded and analyzed. Meanwhile, the diffraction patterns of MgO nanoparticles and modified MgO nanoparticles were measured by XRD (X-Pert PRO MPD, Germany), which could yield the structural morphology of nanoparticles. The diffraction angle varied from 5 to 70° at a rate of 10°/min.

2.3. Preparation of Nanofluids. Instead of a traditional ultrasonic oscillation method, the modified MgO nanofluid was prepared by mechanical grinding technology. This method was mainly completed in the stirred media mill, which consisted of a stainless stirred vessel, a mill chamber, and a pumping system. First, the modified MgO nanoparticles and deionized water were added in the premixed chamber, and then the mixture was pumped to the mill chamber. The milled nanofluid returned to the mixing chamber. The process circulated for 2 h. After continuous reflux, 1000 mL of the modified MgO nanofluid (5 wt %) was fabricated at one time. Then, the modified MgO nanofluid was diluted to needed concentrations by simple mixing (1−5 wt % in this experiment). The structure diagram of the stirred media mill is shown in Figure 2. In contrast, the micrometer MgO slurry, MgO nanofluids of same concentrations were prepared by this method.

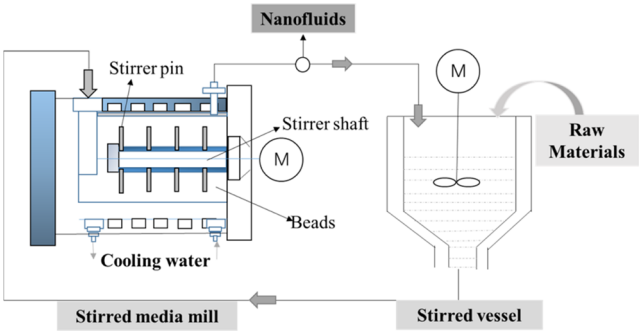

Figure 2. Structure diagram of the improved two-step fabrication of MgO desulfurizers.

2.4. Test of the Suspension Property. First, the states of three MgO desulfurizers with 5 wt % after being placed for different days were recorded. The average particle size of three MgO nanofluids with 5 wt % was measured using a laser diffraction particle size analyzer (Malvern, MS3000). The ζ potential value could be used to predict the suspension characteristics of solid−liquid mixtures. Hence, the ζ potential values of three MgO desulfurizers were measured using a ζ potential instrument (Brookhaven Instruments Corporation). The sedimentation rate was an index that could qualitatively evaluate the stability of solid−liquid mixtures, which could be calculated by eq 1:

$$P_t = \frac{\Delta\varphi}{\varphi_0} = \frac{\varphi_0 - \varphi_t}{\varphi_0} \quad (1)$$

where φ_0 and φ_t represent the mass concentrations of MgO desulfurization slurries before and after standing for a given time. The method is to use a thermal analyzer to measure the concentration of the supernatant in the mixture. The supernatant is taken as a sample and heated to 1000 °C at the rate of 10 °C per minute in an argon atmosphere, and then the solid content of the slurry is obtained by analyzing the thermogravimetric spectrum.

2.5. Desulfurization Experiments and Dissolution Behavior. The diagram of the flue gas desulfurization device can be seen in Figure 3. The bubbling column was 6 cm in diameter and 50 cm in height. The concentration of the MgO desulfurizer used for desulfurization was 5 wt %. A mixture of SO_2, O_2, and N_2 was used to simulate flue gas. The mixture contained O_2 of 4%, which could oxidize the desulfurization product $MgSO_3$ to $MgSO_4$ partially. The volume of SO_2 in the flue gas simulation was 1000 ppm, and the gas flow rate of the desulfurization device was 2 L/min. The same amount of different kinds of MgO desulfurizers was added into the bubble column to evaluate their desulfurization effect. The whole desulfurization reaction was controlled at 30 °C in a thermostatic water bath. The pH of the desulfurizer and the

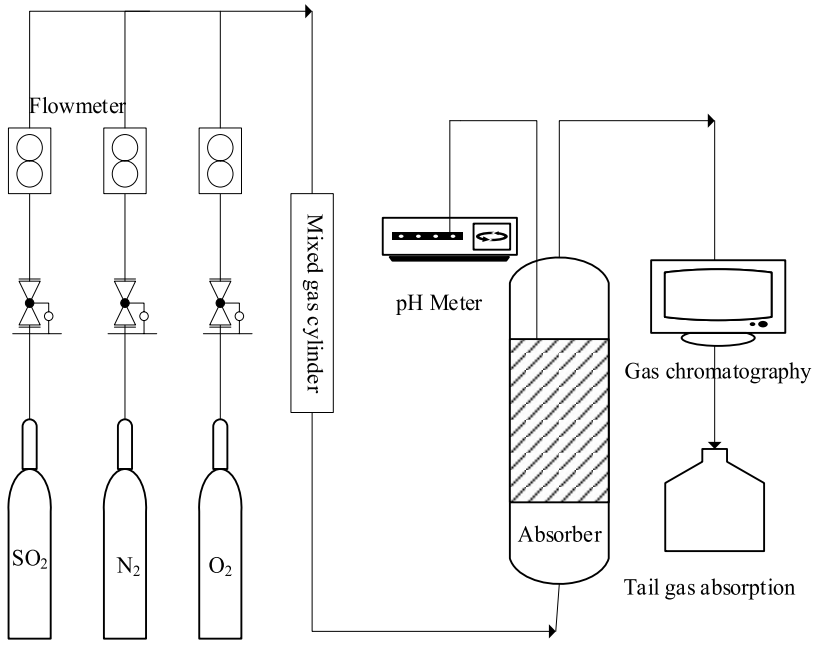

Figure 3. Flow diagram of the flue gas desulfurization device.

https://doi.org/10.1021/acsomega.3c08575
ACS Omega 2024, 9, 12779−12788

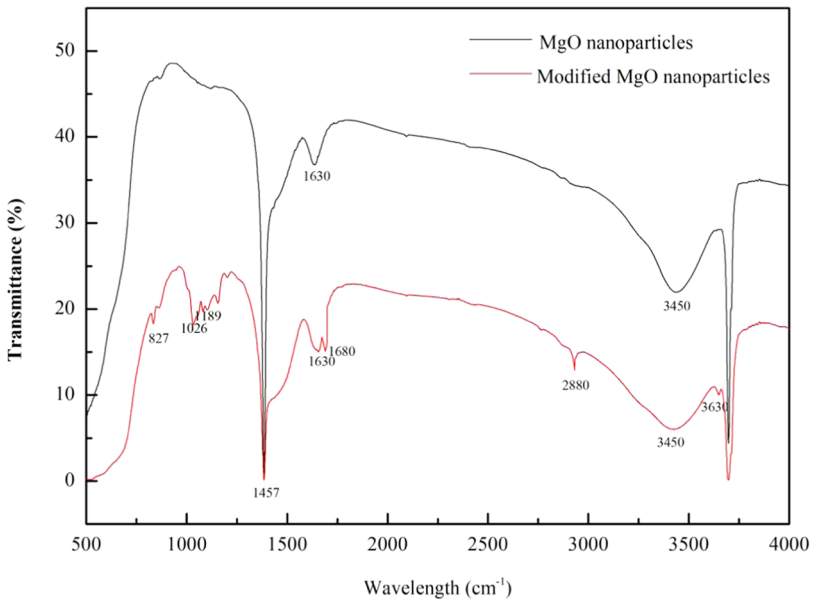

Figure 4. FTIR spectra of MgO nanoparticles and modified MgO nanoparticles.

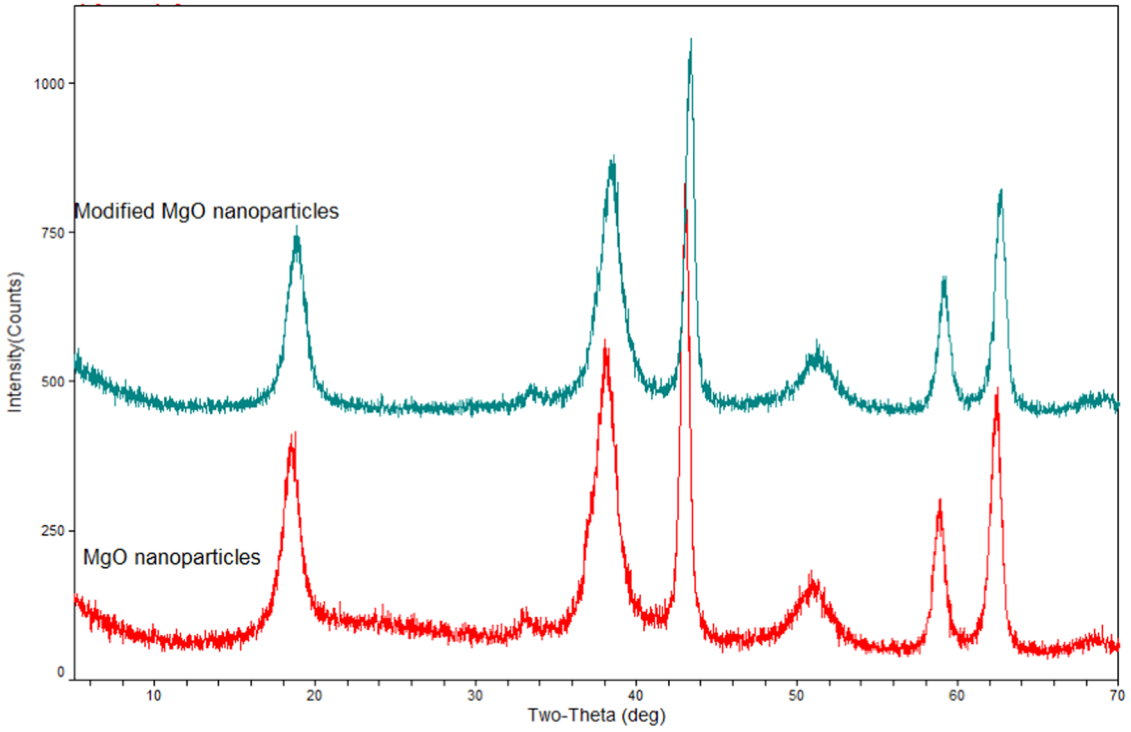

Figure 5. XRD patterns of MgO nanoparticles and modified MgO nanoparticles.

concentration of SO_2 in the off-gas during desulfurization were measured by pH probe and gas chromatography, respectively. The desulfurization breakthrough curves of the desulfurizers were plotted by measuring the concentration of H_2S in the exhaust gas (C) and the concentration of H_2S in the inlet (C_0).

The dissolution of MgO particles is an important rate-determining step in the entire process of desulfurization. The dissolution rate of the MgO desulfurizer could be obtained by measuring the concentration of Mg^{2+} in the solution during the desulfurization process, instead of using the original pH-stat method to measure the dissolution rate of the desulfurizer. Inductively coupled plasma luminescence spectrometry (Agilent ICPOES 730) was used to quantitatively determine Mg^{2+} in desulfurization suspensions at different times. The conversion rate could be obtained by calculating the ratio of the content of Mg^{2+} in the desulfurizer at different times to the total content of Mg^{2+} in the desulfurizer.

3. RESULTS AND DISCUSSION

3.1. Characterization of Modified MgO Nanoparticles.

The FTIR spectra of MgO nanoparticles and modified MgO nanoparticles are depicted in Figure 4. The absorption peak of the modified MgO nanoparticles at 3400−3500 cm^{-1} was broader than that of the MgO nanoparticles; it was mainly

https://doi.org/10.1021/acsomega.3c08575
ACS Omega 2024, 9, 12779−12788

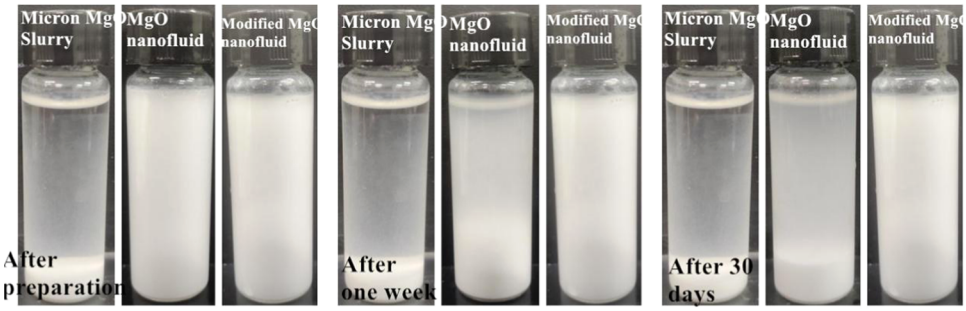

Figure 6. Digital photograph of MgO desulfurizers after different days of standing.

caused by the stretching vibration of −OH. A large amount of −OH was introduced through β-cyclodextrin during the modification of the nanoparticles. The weak absorption peak at 3630 cm^{-1} might be the N−H stretching vibration. The absorption peak at 2880 cm^{-1} was a symmetric stretching vibration peak of $-CH_2-$. The stretching vibration peak with C═O appeared at 1680 cm^{-1}. The stretching vibration peaks of the Si−O bond appeared at 827 and 1189 cm^{-1}, respectively. Compared with the spectrogram of MgO nanoparticles, the characteristic peaks of −OH, $-CH_2-$, Si−O, and C═O appeared in the spectrogram of modified MgO nanoparticles, indicating that β-CD was successfully attached to the surface of MgO nanoparticles.

Figure 5 reveals the XRD patterns of the two kinds of nanoparticles. The two samples had significant characteristic diffraction at 2θ values of 18, 38, 43, 51, 59, and 62. The XRD patterns of modified MgO nanoparticles and MgO nanoparticles did not show significant differences, indicating that the modification of MgO nanoparticles did not substantially change the crystal structure of the nanoparticles.

3.2. Suspension Properties. The suspension stability of the MgO desulfurizer is not only convenient for storage but also its good dispersion is conducive to its rapid dissolution in the desulfurization process. Static sedimentation experiments could intuitively show the suspension stability of different kinds of MgO desulfurizers. It can be seen from Figure 6 that the micron MgO slurry had completely precipitated after preparation because of its large weight. The MgO nanofluid appeared precipitated with 1 week of preparation and totally precipitated with a standing of 30 days. But the modified MgO nanofluid still had no precipitation or stratification after 30 days, showing excellent stability. Then, the unmodified MgO nanofluid agglomerated rapidly, while the modified MgO nanofluid changed little with time, which showed that the modification of the hydrophilic functional groups was conducive to long-term stability.

In order to predict the long-term stability of the MgO desulfurizer, the ζ potential values of the above two nanofluids were measured. As shown in Figure 7, the ζ potential of the modified MgO nanofluid prepared by mechanical grinding technology was still greater than 50 mV after 30 days of placement, while the ζ potential of the MgO nanofluid dropped rapidly during placement, and the ζ potential value was only 21.7 mV after 30 days of placement. Through comparison, it was found that the experimental results of the ζ potential were consistent with the static settlement method, while in the process of preparing nanofluids by mechanical grinding technology, the large contact area and impact force between the stirring medium in the grinding room and the nanoparticles made the nanoparticles fully dispersed. Meanwhile, after being modified, the van der Waals force and the hydrogen bond between the hydrophilic group and the basefluid as well as the large steric resistance of cyclodextrin could maintain good dispersion between the nanoparticles and good stability of the nanofluids.

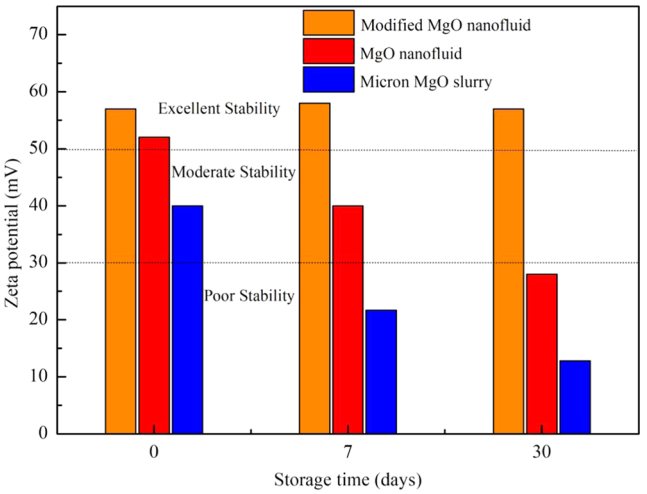

Figure 7. ζ Potential of MgO desulfurizers after different days of standing.

Meanwhile, considering the application of MgO nanofluids, the settling rate was measured to quantitatively determine the suspension property of the modified MgO desulfurizer. The settling rates of modified MgO nanofluids with various concentrations obtained by the improved two-step method are shown in Figure 8. The settling rates of all concentrations of MgO nanofluids after 30 days were less than 7%, of which the sedimentation rate of 1 wt % modified MgO was 3.53% and the settling rate of 5 wt % nanofluids was 6.88%. It indicated that the MgO desulfurizer prepared by this method could have good dispersion for a long time, which had potential application in the field of flue gas desulfurization. Moreover, compared with the traditional preparation method of nanofluids, mechanical grinding technology has certain advantages. First, through the experimental data, it could be seen that nanofluids prepared by this method had good dispersion and stability. Second, this method had no redundant steps in the preparation process, which was easy to operate. Finally, the size of the stirred media mill used in industrial production could be expanded to facilitate the preparation of large-scale industrial nanofluids.

3.3. Dissolution Kinetics of Different MgO Desulfurizers. It was essential to study the dissolution kinetics of different kinds of MgO desulfurizers, as the release capacity of

https://doi.org/10.1021/acsomega.3c08575
ACS Omega 2024, 9, 12779−12788

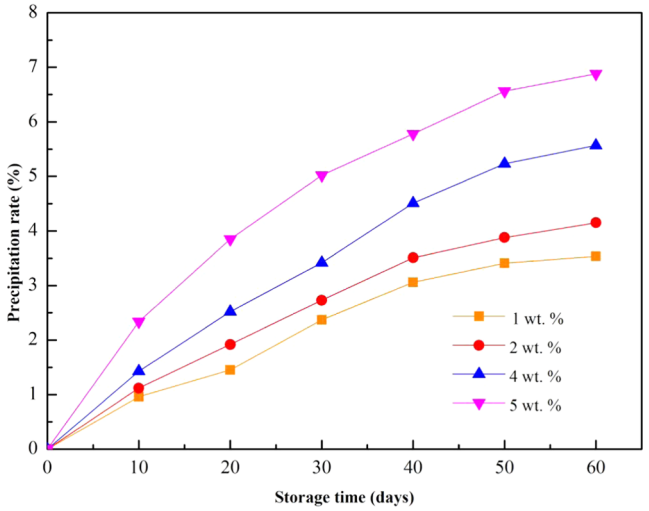

Figure 8. Settling rates of modified MgO nanofluids prepared by mechanical grinding technology with different concentrations.

Mg^{2+} was an important factor to evaluate the effect of MgO desulfurizers on the absorption of SO_2. Figure 9 describes the conversion curves of MgO desulfurizers in the actual desulfurization process. As observed, the dissolution rate of the micron MgO slurry was the slowest, which took 700 min. The dissolution rate of the MgO nanofluid prepared by different methods was significantly faster than that of the micron MgO slurry. Obviously, the smaller the particle size of the desulfurizer, the stronger was the release ability of Mg^{2+}. From the suspension characteristic experiment, we could see that nanoparticles in the unmodified MgO nanofluid would agglomerate to different degrees, resulting in a larger average particle size. While the modified MgO nanofluid had good dispersion, the large gas−liquid contact area was conducive to a greater mass transfer flux of H^+, which could promote the dissolution of the MgO desulfurizer.

Moreover, the main reaction of wet desulfurization by MgO desulfurizers was that MgO first combined with water to generate $Mg(OH)_2$, and $Mg(OH)_2$ further removed SO_2 to complete the desulfurization process (as shown in eq 2 and 3). However, due to the low solubility of MgO in water, hydrophilic groups were introduced on the surface of modified MgO nanoparticles, which increased the affinity between the MgO desulfurizer and water and promoted the process of the MgO desulfurizer transforming into $Mg(OH)_2$. The dissolution rate of the MgO desulfurizer was further enhanced.

$$MgO + H_2O = Mg(OH)_2 \quad (2)$$

$$Mg(OH)_2 + SO_2 = MgSO_3 + H_2O \quad (3)$$

In order to further understand and discuss the dissolution kinetics of the MgO desulfurizer, the core shrinking model was used to analyze the dissolution rate. As the desulfurization product was $MgSO_4$, there was no solid inert residue, and so the particles would continue to shrink and eventually disappear. Therefore, the whole desulfurization process was only affected by the diffusion of the fluid retention film and the chemical reaction rate. As the solid particles of the MgO desulfurizer kept shrinking, the mass transfer coefficient of the fluid retention membrane was affected by particle size and the fluid flow rate. The relationship between conversion and reaction time is obtained as follows:

$$t/t_f = 1 - (R_C/R_S)^2 = 1 - (1 - x_B)^{2/3} \quad (4)$$

The whole reaction is controlled by a chemical reaction:

$$t/t_f = 1 - R_C/R_S = 1 - (1 - x_B)^{1/3} \quad (5)$$

The conversion rate, as shown in Figure 9, was analyzed by the fluid retention film diffusion control models and the chemical reaction control models to calculate the kinetics and reaction parameters. Figures 10 and 11 show the results of the conversion rate fitting with eqs 4 and 5, respectively.

Obviously, for the micrometer slurry, the dissolution rate was mainly controlled by the chemical reaction on the particle surface. This was because the specific surface area of the micrometer MgO particles was small, which led to the smaller

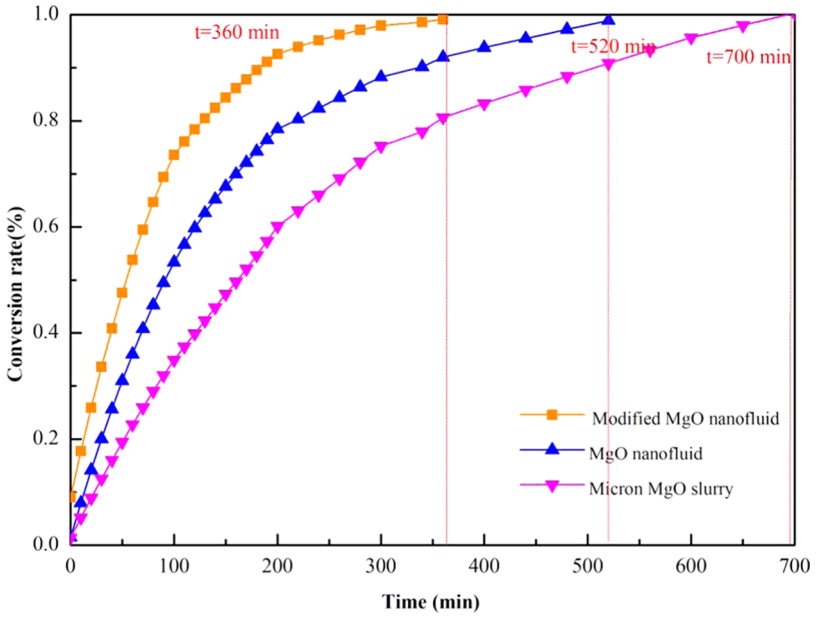

Figure 9. Conversion−time curves obtained for MgO desulfurizers.

https://doi.org/10.1021/acsomega.3c08575
ACS Omega 2024, 9, 12779−12788

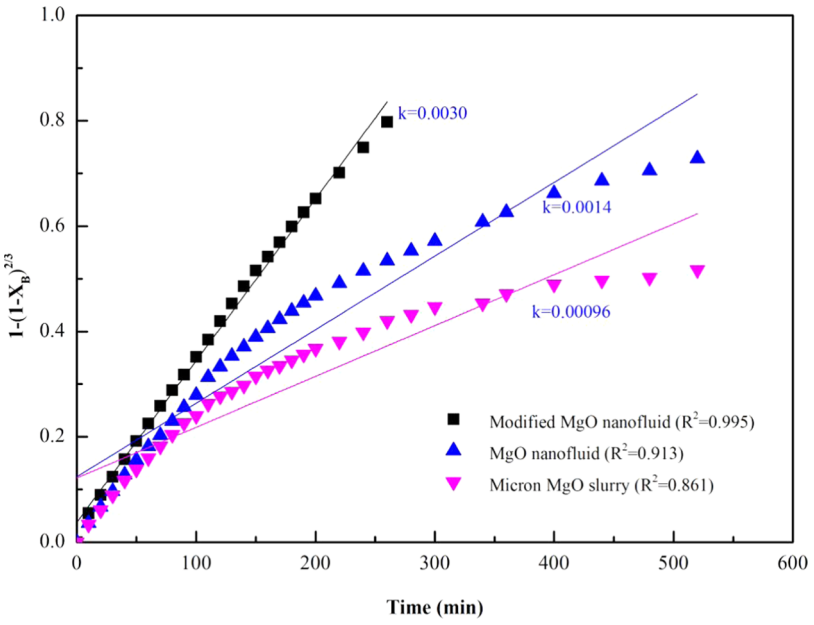

Figure 10. Relation between $1-(1-X_B)^{2/3}$ and the reaction time of MgO desulfurizers.

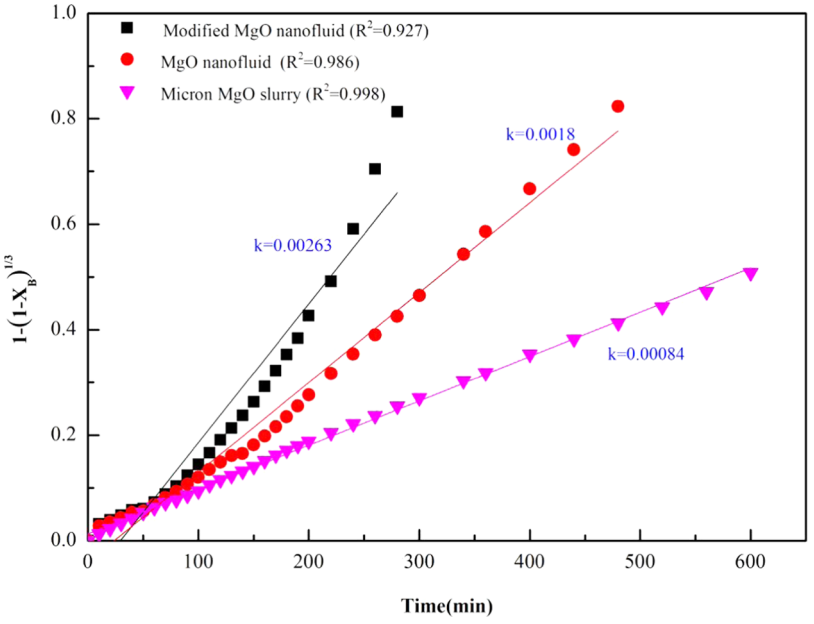

Figure 11. Relation between $1-(1-X_B)^{1/3}$ and the reaction time of MgO desulfurizers.

contact area with the solution. Hence, the dissolution process of the particles was mainly affected by the reaction rate with H^+ in the solution under the same concentration of H^+. However, due to the agglomeration of MgO nanoparticles, the particle size of the MgO nanofluid was larger, and the chemical reaction was still the speed control step in the whole dissolution process. Meanwhile, compared with MgO nanofluids, modified MgO nanofluids fabricated with the improved two-step method were more dispersed among particles and had a larger contact area with the solution. The reaction speed of H^+ and MgO was fast, and the consumed H^+ needed to be supplemented in large quantities. The entire dissolution process was mainly controlled by liquid film diffusion.

The dissolution rate constants of the three MgO desulfurizers could be calculated from the linear slope obtained from the linear regression between dissolution conversion and reaction time. It could be seen that the dissolution rate constant ranged from 0.00084 to 0.0030 min^{-1}, which increased with the decrease of particle size and the increase of particle dispersion. Meanwhile, the Arrhenius law was used to further understand the dissolution kinetics of MgO desulfurizers, which are shown as eqs 6 and 7.

$$k = k_0 e^{-E/RT} \tag{6}$$

$$\ln k = \ln k_0 - \frac{E}{RT} \tag{7}$$

Therefore, we could obtain the activation energy required for desulfurization by a MgO desulfurizer by measuring the relationship between the dissolution rate constant and

https://doi.org/10.1021/acsomega.3c08575
ACS Omega 2024, 9, 12779−12788

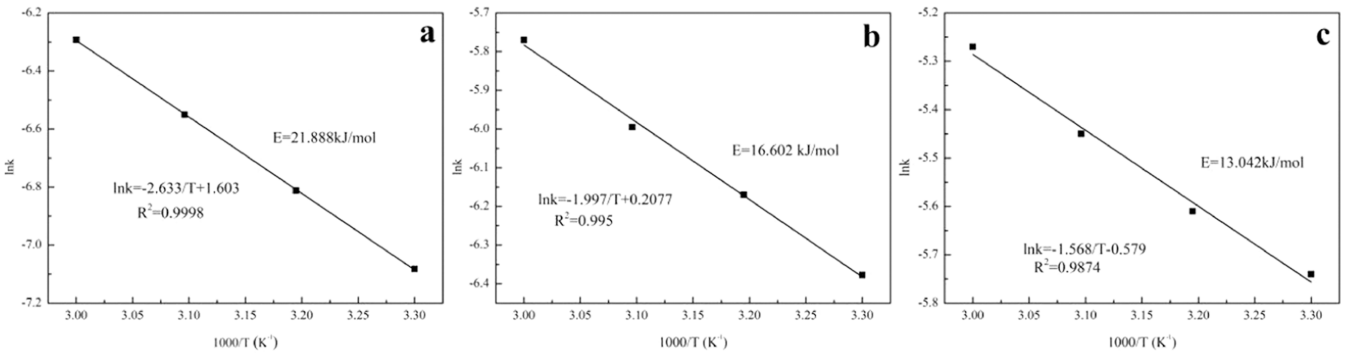

Figure 12. Dissolution rate constant versus temperature: (a) MgO slurry, (b) MgO nanofluid, and (c) modified MgO nanofluid.

temperature. The dissolution rate constants of three MgO desulfurizers at the temperature of 30 to 60 °C were measured, and the apparent activation energy required for desulfurization was calculated according to eq 7, which is shown in Figure 12. The apparent activation energy required for the micrometer MgO desulfurizer was 21.888 kJ/mol. However, with the decrease of particle size and the increase of the gas−liquid contact area, the apparent activation energy required for desulfurization was reduced. The apparent activation energies of the MgO nanofluid and the modified MgO nanofluid in the desulfurization process were 16.602 and 13.042 kJ/mol, respectively. From the data of the apparent activation energy, it could also be seen that the dissolution process of the modified MgO nanofluid prepared was mainly controlled by liquid film diffusion, which was consistent with the conclusion of Pinna et al.[37]

3.4. Desulfurization Effect of MgO Desulfurizers. The desulfurization breakthrough curves of three desulfurizers are shown in Figure 13. It was considered that the purification

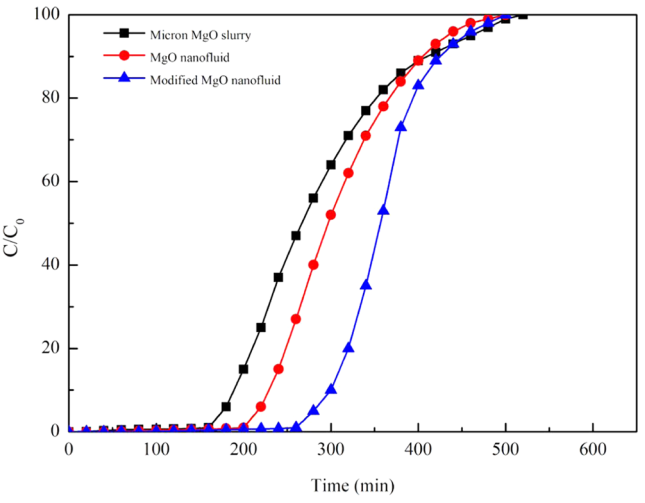

Figure 13. Desulfurization breakthrough curves of the MgO desulfurizers.

degree of SO_2 met the desulfurization requirements as the content of SO_2 in the off-gas was lower than 10 ppm, that is, C/C_0 was less than 1%. It showed that at the beginning of desulfurization, the desulfurization effect of all three desulfurizers could meet the requirements. As the desulfurization reaction proceeded, the MgO slurry reached the penetration earliest, and the penetration time was 162 min. For MgO nanofluids and modified MgO nanofluids, the penetration times were 195 and 238 min, respectively. And with the prolongation of the desulfurization time, the concentration of SO_2 in the tail gas increased sharply. The slope of the breakthrough curve of the MgO slurry was the smallest, while the slope of the breakthrough curve of the modified MgO nanofluid was the largest. This was because of the reduction of particle size and the increase of dispersion of the MgO desulfurizer. The dissolution rate of the desulfurizer was accelerated (as shown in Section 3.3), and the desulfurization ability of the desulfurizer was improved, thus extending the penetration time and accelerating the consumption of the desulfurizer.

The variations of pH of three MgO desulfurizers during desulfurization are shown in Figure 14. The dissolution of MgO particles made the initial pH of the three desulfurizers almost the same. In the alkaline environment, the dissolution of MgO was inhibited, while the pH value started to drop sharply with the introduction of SO_2. It could be seen that the pH−time curves showed different trends. For the MgO slurry and MgO nanofluids, the pH of the solution showed a rapid decline trend because of the slow dissolution rate of the desulfurizers. As the pH values were reduced to 4.2 and 4.5, respectively, the acid solution would inhibit the continued dissolution of SO_2, which inhibited the gas film diffusion. Meanwhile, the acidic environment would accelerate the dissolution rate of the MgO desulfurizer. Both of these made the decline rate of pH slow down until the MgO desulfurizer was consumed, and the pH of the solution would not change anymore. The initial pH values of the modified MgO nanofluids also decreased rapidly. However, with the progress of desulfurization, the decrease of the pH value was slower than that of the unmodified MgO nanofluid. This was due to the better dispersion and hydrophilicity of the modified MgO nanoparticles, which made their dissolution faster. Meanwhile, the higher pH value was conducive to the dissolution of SO_2, reducing the liquid film resistance and further promoting the desulfurization process, which was consistent with the conclusion of the desulfurization experiment.

4. CONCLUSIONS

In this paper, hydrophilic functional groups were introduced on the surface of nanoparticles to improve the stability and dispersion of the MgO desulfurizer so as to promote its dissolution rate and desulfurization efficiency, and its dissolution mechanism was analyzed by the shrinking core model. In order to realize the large-scale industrial application of nanofluids, the traditional two-step method of preparing

https://doi.org/10.1021/acsomega.3c08575
ACS Omega 2024, 9, 12779−12788

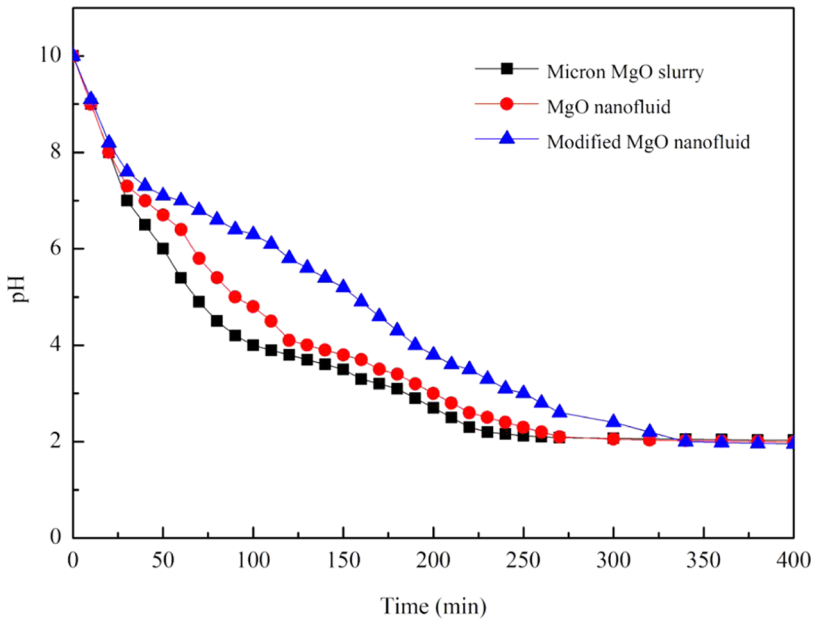

Figure 14. Variations of pH of the solution during desulfurization with the MgO desulfurizers.

nanofluids was improved using wet grinding technology. The conclusions were as follows:

(1) Through static sedimentation, ζ potential measurement, and settling rate measurement, it was shown that the modified MgO nanofluids prepared by wet grinding technology had good stability and dispersion. After 30 days of storage, the ζ potential value still exceeded 50 mV, and the settling rate of the modified nanofluids with 5 wt % was less than 7%.

(2) The modified MgO nanofluids prepared by the improved method could promote the conversion of MgO into $Mg(OH)_2$ and could further promote its dissolution rate due to their good dispersibility and hydrophilicity. From the dissolution kinetics study, it was found that the smaller the particle size of the MgO desulfurizer and the better the dispersibility and hydrophilicity, the lower is the activation energy required for the desulfurization process.

(3) The faster dissolution rate made the pH of the solution decrease slowly, promoted the dissolution of SO_2, reduced the liquid film mass transfer resistance, and prolonged the penetration time to 238 min.

AUTHOR INFORMATION

Corresponding Author

Mengyu Ma − *School of Chemistry and Pharmaceutical Engineering, Huanghuai University, Zhumadian 463000, P. R. China;* orcid.org/0000-0002-8766-0591; Email: mengyumahuagong@126.com

Authors

Hongge Zhao − *School of Chemistry and Pharmaceutical Engineering, Huanghuai University, Zhumadian 463000, P. R. China*

Peng Hu − *School of Chemistry and Pharmaceutical Engineering, Huanghuai University, Zhumadian 463000, P. R. China*

Complete contact information is available at: https://pubs.acs.org/10.1021/acsomega.3c08575

Notes

The authors declare no competing financial interest.

ACKNOWLEDGMENTS

The authors acknowledge the financial support of the Programs for Science and Technology Development of Henan Province [202102210255, 222102320377].

REFERENCES

(1) Chen, Z.; Wang, H. M.; Zhuo, J. K.; You, C. F. Enhancement of mass transfer between flue gas and slurry in the wet flue gas desulfurization spray tower. *Energy Fuels* **2018**, *32*, 703−712.

(2) Zheng, C. H.; Wang, L.; Zhang, Y. X.; Zhang, J.; Zhao, H. T.; Zhou, J. S.; Gao, X.; Cen, K. F. Partitioning of hazardous trace elements among air pollution control devices in ultra-low-emission coal-fired power plants. *Energy Fuels* **2017**, *31*, 6334−6344.

(3) Erans, M.; Jeremias, M.; Zheng, L.; Yao, J. G.; Anthony, E. J.; et al. Pilot testing of enhanced sorbents for calcium looping with cement production. *Appl. Energy* **2018**, *225*, 392−401.

(4) Guerras, L. S.; Martín, M. Optimal gas treatment and coal blending for reduced emissions in power plants: a case study in Northwest Spain. *Energy* **2019**, *169*, 739−749.

(5) Chen, C.; Ma, F.; He, S.; et al. Improved water and efflorescence resistance of flue gas desulfurization gypsum-based composites by generating hydrophobic coatings. *J. Cleaner Prod.* **2022**, *371*, No. 133711.

(6) Chen, X.; Sun, P.; Cui, L.; et al. Limestone-based dual-loop wet flue gas desulfurization under oxygen-enriched combustion. *Fuel* **2022**, *322*, No. 124161.

(7) Tian, H.; Wan, D.; Che, Y.; Chang, J.; et al. Simultaneous magnesia regeneration and sulfur dioxide generation in magnesium-based flue gas desulfurization process. *J. Cleaner Prod.* **2021**, *284*, No. 124720.

(8) Li, X.; Han, J.; Liu, Y. Summary of research progress on industrial flue gas desulfurization technology. *Sep. Purif. Technol.* **2021**, *281*, No. 119849.

(9) Guo, L.; Liu, W. F.; Tang, X. J.; Wang, H.; Liu, Q.; Zhu, Y. M. Reaction kinetics of none-catalyzed jet aeration oxidation of magnesium sulfifite. *Chem. Eng. J.* **2017**, *330*, 870−879.

https://doi.org/10.1021/acsomega.3c08575
ACS Omega 2024, 9, 12779−12788

(10) Luo, Z.; Peng, J. J.; Wang, D. H.; Yang, J. Recovery of phosphate from piggery biogas slurry by ultrasonication, aeration and addition of MgO desulfurization waste residue. *J. Cleaner Prod.* **2019**, *211*, 865−873.
(11) Guo, R.-t.; Pan, W.; Zhang, X.; Xu, H.; Ren, J. Dissolution rate of magnesium hydrate for wet flue gas desulfurization. *Fuel* **2011**, *90*, 7−10.
(12) del Valle-Zermeño, R.; Formosa, J.; Aparicio, J. A.; Guembe, M.; Chimenos, J. M. Transposition of wet flue gas desulfurization using MgO by-products: From laboratory discontinuous batch reactor to pilot scrubber. *Fuel Process. Technol.* **2015**, *138*, 30−36.
(13) Gu, S.; Yang, Z.; Chen, Z.; You, C. Dissolution reactivity and kinetics of low-grade limestone for wet flue gas desulfurization. *Ind. Eng. Chem. Res.* **2020**, *59*, 14242−14251.
(14) Xiang, G.; Gao, R. T.; Ding, H. L.; Luo, Z. Y.; Cen, K. F. Dissolution rate of limestone for wet flue gas desulfurization in the presence of sulfite. *J. Hazard. Mater.* **2009**, *168*, 1059−1064.
(15) Chen, Z.; You, C. F.; Wang, H. M.; Liu, Q. X. Experimental study on the synergetic removal of fine particles by wet flue gas desulfurization tower with a flow pattern control device. *Powder Technol.* **2019**, *343*, 122−128.
(16) Li, W.; Zou, C. Deep desulfurization of gasoline by synergistic effect of functionalized β-CD-TiO_2-Ag nanoparticles with ionic liquid. *Fuel* **2018**, *227*, 141−149.
(17) Dong, X.; Liu, X.; et al. Effect of nanoparticles on desulfurization/regeneration performance of deep eutectic solvent based nanofluid system. *Sep. Purif. Technol.* **2022**, *300*, No. 121875.
(18) Liu, X.; Zhang, Y.; et al. The effect of ZIF-67 nanoparticles on the desulfurization performance of deep eutectic solvent based nanofluid system. *J. Hazard. Mater.* **2022**, *426*, No. 128098.
(19) Zou, Y.; Zhu, W.; et al. Scalable and facile synthesis of V_2O_5 nanoparticles via ball milling for improved aerobic oxidative desulfurization. *Green Energy Environ.* **2021**, *6*, 169−175.
(20) Ma, M.; Zou, C. Effect of nanoparticles on the mass transfer process of removal of hydrogen sulfide in biogas by MDEA. *Int. J. Heat Mass Transfer* **2018**, *127*, 385−392.
(21) Ma, M.; Zou, C. Enhancement by SiC Nanoparticles of the Removal of Hydrogen Sulfide from Natural Gas by a Traditional Desulfurizer. *Energy Fuels* **2017**, *31*, 8054−8060.
(22) Fallah, R. N.; Azizian, S. Rapid and facile desulphurization of liquid fuel by carbon nanoparticles dispersed in aqueous phase. *Fuel* **2012**, *95*, 93−96.
(23) Olajire, A. A.; Abidemi, J.; Lateef, A.; et al. Adsorptive desulphurization of model oil by Ag nanoparticles modified activated carbon prepared from brewer's spent grains. *J. Environ. Chem. Eng.* **2017**, *5*, 147−159.
(24) El Naggar, M. A. A.; Mostafa, M. S.; Zaky, M. T.; et al. New trend for the pour point depression of a waxy petroleum fraction with in-situ desulphurization using (O_2H & OH) radicals coupled with nanoparticles of titanium compounds. *Fuel* **2016**, *180*, 218−227.
(25) Amal, S. A.; Khidr, F. S.; Soliman, T.; Zaki, D. Y.; Sabry, A. M.; Al-Sabagh. Adsorptive removal of thiophene by using water based silver nanofluid. *Fuel* **2023**, *334*, No. 126584.
(26) Schilde, C.; Breitung-Faes, S.; Kampen, I.; Kwade, A. Grinding kinetics of nano-sized particles for different electrostatic stabilizing acids in a stirred media mill. *Powder Technol.* **2013**, *235*, 1008−1016.
(27) Kumar, R. S.; Chaturvedi, K. R.; Iglauer, S.; et al. Impact of anionic surfactant on stability, viscoelastic moduli, and oil recovery of silica nanofluid in saline environment. *J. Pet. Sci. Eng.* **2020**, *195*, No. 107634.
(28) Karami, M.; Akhavan Bahabadi, M. A.; Delfani, S.; Ghozatloo, A. A new application of carbon nanotubes nanofluid as working fluid of low-temperature directabsorption solar collector. *Sol. Energy Mater. Sol. Cells* **2014**, *121*, 114−118.
(29) Said, Z.; Allagui, A.; Abdelkareem, M. A.; Alawadhi, H.; Elsaid, K. Acid-functionalized carbon nanofibers for high stability, thermo-electrical and electrochemical properties of nanofluids. *J. Colloid Interface Sci.* **2018**, *520*, 50−57.
(30) Xian, H. W.; Azwadi Che Sidik, Nor.; Saidur, R. Impact of different surfactants and ultrasonication time on the stability and thermophysical properties of hybrid nanofluids. *Int. Commun. Heat Mass Transfer* **2020**, *110*, No. 104389.
(31) Choudhary, R.; Khurana, D.; Kumar, A.; et al. Stability analysis of Al_2O_3/water nanofluids. *J. Exp. Nanosci.* **2017**, *12*, 140−151.
(32) Murshed, S. M. S.; Castro, C. A. N. D. Conduction and convection heat transfer characteristics of ethylene glycol based nanofluids−a review. *Appl. Energy* **2016**, *184*, 681−695.
(33) Masaaki, E. Current pigment dispersion for the paint and the dispersion process. *Shikizai Kyokaishi* **2014**, *87*, 204−208.
(34) Zhao, L. H.; He, L.; He, B. H. Effect of dispersants pre-adsorption and grinding on dispersion performance of kaolin pigment. *Adv. Mater. Res.* **2013**, *748*, 41−45.
(35) Bilgili, E.; Hamey, R.; Scarlett, B. Nano-milling of pigment agglomerates using a wet stirred media mill: elucidation of the kinetics and breakage mechanisms. *Chem. Eng. Sci.* **2006**, *61*, 149−157.
(36) Celep, O.; Aslan, N.; Alp, I.; Taşdemir, G. Optimization of some parameters of stirred mill for ultra-fine grinding of refractory Au/Ag ores. *Powder Technol.* **2011**, *208*, 121−127.
(37) Pinna, E. G.; Drajlin, D. S.; Toro, N.; Rodriguez, M. H. Kinetic modeling of the leaching of $LiCoO_2$ with phosphoric acid. *J. Mater. Res. Technol.* **2020**, *9*, 14017−14028.

https://doi.org/10.1021/acsomega.3c08575
ACS Omega 2024, 9, 12779−12788